Available online at www.sciencedirect.com
ScienceDirect
Journal of Crystal Growth 299 (2007) 288–294
JOURNAL OF CRYSTAL GROWTH
www.elsevier.com/locate/jcrysgro

# Epitaxial growth of biferroic $YMnO_3(0\,0\,0\,1)$ on platinum electrodes

X. Martí[a,*], F. Sánchez[a], D. Hrabovsky[a], J. Fontcuberta[a], V. Laukhin[a,b], V. Skumryev[b,c], M.V. García-Cuenca[d], C. Ferrater[d], M. Varela[d], U. Lüders[e], J.F. Bobo[e], S. Estradé[f], J. Arbiol[f], F. Peiró[f]

[a]*Institut de Ciència de Materials de Barcelona—CSIC, Campus U.A.B., Bellaterra 08193, Spain*
[b]*Institut Català de Recerca i Estudis Avançats (ICREA), Barcelona, Spain*
[c]*Departament de Física, Universitat Autònoma de Barcelona, Bellaterra 08193, Spain*
[d]*Departament de Física Aplicada i Òptica, Universitat de Barcelona, Diagonal 647, Barcelona 08028, Spain*
[e]*LNMH CNRS-ONERA, BP 4025, 31055 Toulouse Cedex 4, France*
[f]*Departament d'Electrònica, Universitat de Barcelona, Diagonal 647, Barcelona 08028, Spain*

Received 21 August 2006; accepted 8 November 2006
Communicated by D.P. Norton
Available online 19 December 2006

**Abstract**

Epitaxial films of the biferroic $YMnO_3$ (YMO) oxide have been grown on platinum-coated $SrTiO_3(1\,1\,1)$ and $Al_2O_3(0\,0\,0\,1)$ substrates. The platinum electrodes, (1 1 1) oriented, are templates for the epitaxy of the hexagonal phase of YMO with a (0 0 0 1) out-of-plane orientation, which is of interest as this is the polarization direction of YMO. X-ray diffractometry indicates the presence of two crystal domains, 60° rotated in-plane, in the Pt(1 1 1) layers which subsequently are transferred on the upperlaying YMO. Cross-section analysis by high-resolution transmission electron microscopy (HRTEM) of $YMnO_3/Pt/SrTiO_3(1\,1\,1)$ shows high-quality epitaxy and sharp interfaces across the structure in the observed region. We present a detailed study of the epitaxial growth of the hexagonal YMO on the electrodes.


*PACS:* 61.68; 70

*Keywords:* A1. X-ray diffraction; A3. Physical vapor deposition processes; B1. Oxides; B2. Magnetoelectric materials; B2. Multiferroic materials

## 1. Introduction

In the recent years, multiferroics appear to open new avenues for the development of novel devices based in new functionalities such as control of the magnetic properties by means of electrical fields and vice versa [1,2]. $YMnO_3$, in its hexagonal phase, is one of the most studied biferroic materials. Ferroelectricity ($T_c$~900 K) and antiferromagnetism ($T_N$~80 K) coexist at low temperature. On one hand, ferroelectricity occurs along [0 0 0 1] axis [3] and, on the other hand, antiferromagnetic coupled manganese magnetic moments are located within the basal plane, forming a geometrically frustrated triangular magnetic network [4]. Due to this arrangement of electrical and magnetic orders, epitaxial growth of (0 0 0 1) textured hexagonal thin films is fundamental towards the development of functional structures. Moreover, towards the integration of ferroelectric YMO into devices, epitaxial films onto suitable bottom electrodes must be developed. Indeed, Ito et al. [5] have earlier reported the epitaxy of $YMO(0\,0\,0\,1)$ films on $Pt(1\,1\,1)/Al_2O_3(0\,0\,0\,1)$. Although the polarization P(E) loops of these films were better that those of polycrystalline YMO films, squarer P(E) loops are required [5]. Film microstructure plays a fundamental role on the ferroelectric properties and detailed structural studies on hexagonal YMO hexagonal films is still lacking.

*Corresponding author.
*E-mail address:* xavi.mr@gmail.com (X. Martí).

0022-0248/$ - see front matter © 2007 Elsevier B.V. All rights reserved.
doi:10.1016/j.jcrysgro.2006.11.272

Recently, polycrystalline hexagonal $YMnO_3$ films of varied crystal texture on silicon substrates were combined with a ferromagnetic layer with the purpose of exploiting the biferroic (ferroelectric and antiferromagnetic) character of YMO [6]. It was observed that the film texture was strongly dependent on the growth conditions, namely the oxygen pressure, but remarkably enough, the films do not display any polarization remanence probably due to the presence of defects.

Here, we will address some of these questions with particular emphasis on the in-plane texture of the films and film/electrode/substrate interfaces. We detail the crystal properties and surface morphology of the epitaxial $YMnO_3$(0 0 0 1) film and the Pt(1 1 1) electrode grown on two different substrates: $SrTiO_3$(1 1 1) and $Al_2O_3$(0 0 0 1). We will disclose the in-plane epitaxial relationships and we will show that in-plane bidomains of YMO always occurs. Our work sheds light on the epitaxy of these bilayers, which constitute a step towards the controlled growth of biferroic oxides on metallic layers for its use in the development of new devices.

## 2. Experimental procedure

As a first step, platinum films were deposited on $SrTiO_3$(1 1 1)—STO(1 1 1) and $Al_2O_3$(0 0 0 1)—ALO (0 0 0 1) substrates by DC sputtering. Before the deposition, the substrates were heated up to 800 °C and, afterwards, Pt was deposited at $5 \times 10^{-3}$ mbar pure Ar and at substrate temperature of 500 °C. Pt films with different thicknesses in the 4–180 nm range were grown at a growth rate of 1.8 nm/min.

Subsequently, $YMnO_3$ films were grown on the platinum electrodes by pulsed laser deposition. A KrF excimer laser (248 nm wavelength, 34 ns pulse duration) was used at a repetition rate of 5 Hz. The laser beam was focused to a fluence around 1.5 J/cm$^2$ on a stoichiometric $YMnO_3$ target, being the substrate placed at a distance of 5 cm. The films were deposited at a substrate temperature of 800 °C in a 0.2 mbar of oxygen pressure. At the end of the growth, the substrate was cooled down and 1 atm of oxygen was introduced in the chamber at 500 °C. $YMnO_3$ films in the range of 90–150 nm thickness were obtained at a rate of 0.12 Å/pulse.

The crystal structure was investigated by X-ray diffractometry (XRD) using Cu $K_\alpha$ radiation. X-ray reflectometry was used to determine the growth rate. The morphology of Pt and $YMnO_3$ films was investigated by atomic force microscopy (AFM) working in dynamic mode. Transmission electron microscopy (TEM) of a YMO/Pt/STO(1 1 1) sample was performed preparing the thin foil specimen in cross-section (XT) geometry by mechanical polishing down to about 30 μm, and then ion beam milling at 5 keV and 7° down to electrotransparency. The sample has been observed in high-resolution (HRTEM) conditions in a Jeol J2010 field emission gun microscope, with an accelerating voltage of 200 kV.

## 3. Results and discussion

In Fig. 1a and b we show the $\theta/2\theta$ scans of the YMO/Pt/ALO(0 0 0 1) and YMO/Pt/STO(1 1 1), respectively. The thickness of the films in these bilayers is 100 nm (YMO) and 15 nm (Pt). Data in Fig. 1 indicate that the Pt films on both substrates have a (1 1 1) texture. $\theta/2\theta$ scans were performed also prior the YMO growth, and data have been used to evaluate the out-of-plane cell parameters of Pt, its evolution with thickness and the effect of subsequent growth of YMO on it. The data, circles in Fig. 2a, (corresponding to Pt/ALO samples) reveal that the out-of-plane parameter undergoes a rapid relaxation as thickness increases, approaching the bulk value ($d_{1\,1\,1} = 2.265$ Å). We also notice that after the growth of YMO, the out-of-plane parameter of the thinnest Pt layers (squares in Fig. 2a) is coincident, within the experimental resolution, with the bulk one. This indicates that during the growth of YMO the Pt underlayer relaxes. Further, Fig. 2b shows a zoom around Pt(1 1 1) peak in reciprocal space units for a Pt/ALO(0 0 0 1) film. Laue oscillations are found to follow the expected $I(q) \sim \sin^2(N \cdot \pi q)/\sin^2(\pi q)$ dependence. By fitting the previous function to the data, film's thickness can be derived. It turns out that for the Pt film of Fig. 2b, $t = 7.0$ nm, which is in good agreement with the thickness estimated from the calibrated growth rate. It is worth mentioning that Laue fringes around the Pt(1 1 1) diffraction peaks of the Pt film on both substrates are also observed (see Fig. 1), even after heating the Pt/substrate to 800 °C as required to grow the YMO films, thus indicating that the quality of the Pt film is preserved.

We also note in Fig. 1 that only (0 0 0 1) reflections corresponding to the hexagonal YMO phase are visible, thus suggesting that the films must have a much

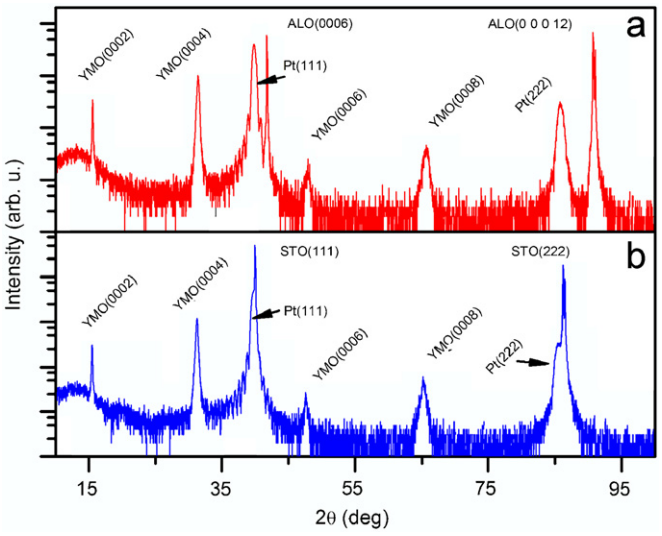


Fig. 1. X-ray diffraction $\theta/2\theta$ scans of $YMnO_3$/Pt bilayers on (a) $Al_2O_3$(0 0 0 1) and (b) $SrTiO_3$(1 1 1) substrates. $YMnO_3$ and Pt films are 100 and 15.8 nm thick, respectively. Note the presence of Laue fringes for the Pt(1 1 1) reflections.

dominating, if not unique, (0 0 0 1) texture. The out-of-plane $c$ lattice parameter of the YMO film on Pt/STO (Fig. 1a) is $c = 11.45$ Å ($\varepsilon_{(0\,0\,0\,1)} = 0.44\%$, calculated as $[d_{(0\,0\,0\,1)\mathrm{exp}} - d_{(0\,0\,0\,1)\mathrm{bulk}}]/d_{(0\,0\,0\,1)\mathrm{bulk}}$), whereas on the Pt/ALO substrate (Fig. 1b), $c = 11.39$ Å which indicates that on this substrate the YMO film is almost fully relaxed. The $\omega$-scans of symmetrical reflections (not shown here) produced relatively narrow rocking curves, with full-width at half-maximum (FWHM) around 0.6° in both substrates. This value is comparable to that reported (~0.7°) by Ito et al. [5] for YMO/Pt/ALO but larger than that measured by Dho et al. [7] for YMO on unbuffered—without an electrode—YSZ(1 1 1) substrates. It reflects that the prepared films on platinum layers should present a substantial spread of out-of-plane directions.

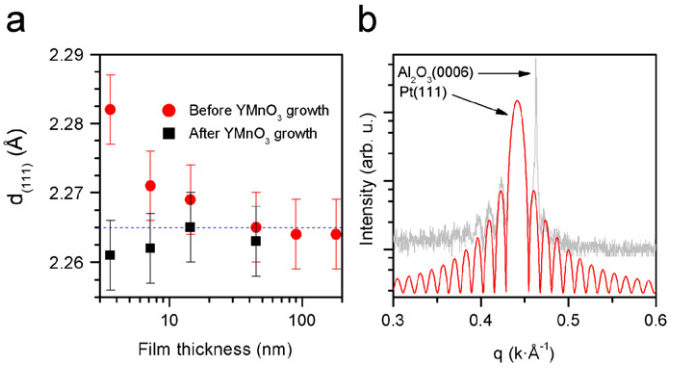


Fig. 2. (a) Dependence of the $d_{(1\,1\,1)}$ out-of-plane parameter of the Pt/$Al_2O_3$(0 0 0 1) films with the thickness. The dashed line represents the bulk value. (b) X-ray diffraction around the Pt(1 1 1) reflection in reciprocal space units of a film on $Al_2O_3$(0 0 0 1), and a fit assuming the Pt film is $t = 7.0$ nm thick.

We turn now to the in-plane structure of the films. The $\phi$-scans are presented in Fig. 3. They indicate that epitaxial growth of YMO(0 0 0 1)/Pt(1 1 1) structures has been achieved on ALO(0 0 0 1) (Fig. 3a) and STO(1 1 1) (Fig. 3b). Firstly, the $\phi$-scan around the ALO(1 0 $\underline{1}$ 4) reflections shows three peaks, 120° spaced, corresponding to the three-fold symmetry of the ALO substrate (Fig. 3a, bottom). The scan around the Pt(2 0 0) reflection (Fig. 3a, center) shows six peaks, 60° spaced. We notice that according to the three-fold symmetry of the Pt(1 1 1) surface, three peaks were expected. This observation indicates the presence of two crystalline Pt domains, 60° in-plane rotated, which had been already reported [8,9] on ALO(0 0 0 1) and STO(1 1 1) substrates. By comparing the position of the peaks in the $\phi$-scans, the epitaxial relationships for both Pt domains are derived: [1 1 $\underline{2}$] Pt/[1 0 $\underline{1}$ 0] ALO and [$\underline{1}$ 1 2] Pt//[1 0 $\underline{1}$ 0] ALO. The $\phi$-scan corresponding to the YMO(1 1 $\underline{2}$ 1) reflections in Fig. 3a (top) shows six peaks. Due to the $YMnO_3$ helicoidal symmetry, six reflections were expected and thus it is not possible to elucidate, from this $\phi$-scan, the eventual presence of one or two YMO domains. However,

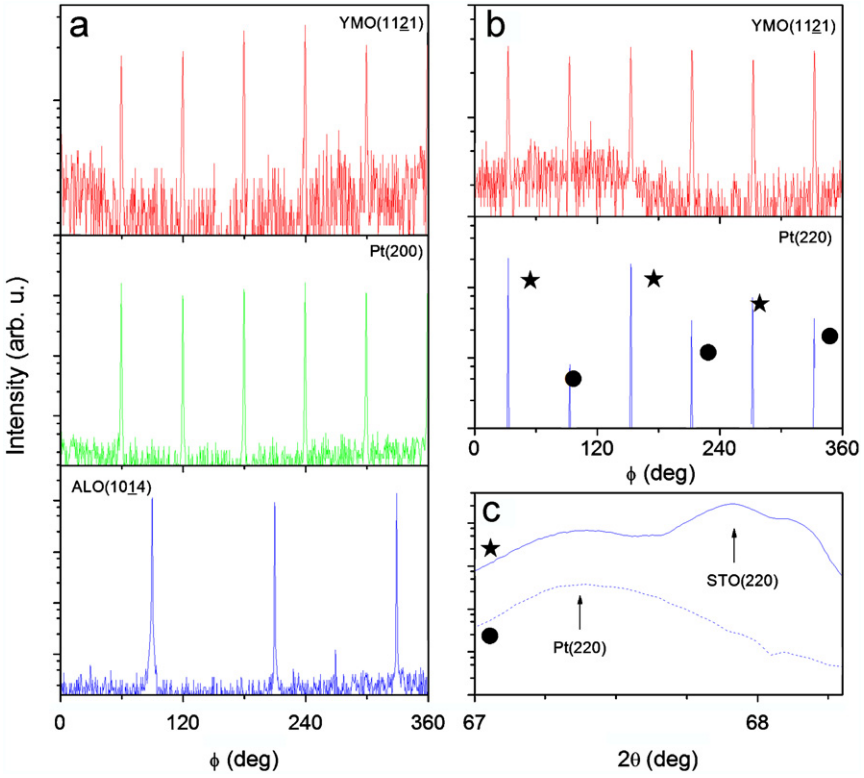


Fig. 3. X-ray diffraction $\phi$-scans indicating the epitaxial growth of $YMnO_3$//Pt on both substrates. (a) For films on $Al_2O_3$ substrates, the scans were around the crystal planes $YMnO_3$(1 1 2 1), Pt(2 0 0), and $Al_2O_3$(1 0 1 4). (b) For films on $SrTiO_3$ substrates, the scans were around the crystal planes: $YMnO_3$(1 1 2 1), and Pt(2 2 0) and $SrTiO_3$(2 2 0). (c) $\theta/2\theta$ scans around asymmetrical Pt(2 2 0) performed at the two $\phi$ positions labelled in Fig. 3b. The scans indicate that starred peaks contain substrate and Pt contributions whereas filled circle peaks contain only Pt contributions.

since there are two domains in the buffering Pt electrode, two domains are also likely to be in the $YMnO_3$ film. The corresponding in-plane epitaxial relationships would be [1 $\bar{1}$ 0 0] $YMnO_3$/[1 $\bar{1}$ 0] Pt and [1 $\bar{1}$ 0 0] $YMnO_3$/[$\bar{1}$ 1 0] Pt.

We now consider the films grown on STO(1 1 1). In Fig. 3b (bottom), we show the $\phi$-scan of the Pt(2 2 0) reflections. The plot shows six peaks and, by careful study using $\theta/2\theta$ scans on each peak (Fig. 3c), it is confirmed that only three peaks contain $SrTiO_3$ contributions, whereas all six peaks contain Pt contributions. Therefore, it indicates that Pt on STO(1 1 1) develops the same domain structure as on ALO(0 0 0 1). The epitaxial relationships for the two domains are [1 $\bar{1}$ 0] Pt/[1 $\bar{1}$ 0] STO and [$\bar{1}$ 1 0] Pt/[1 $\bar{1}$ 0] STO. It is to be noted that in previous reports [10], chemical etching of the STO(1 1 1) substrates was found to be necessary to avoid the presence of additional domains, 30° in-plane rotated. Here, the only treatment of the substrate was an in situ pre-annealing at 800 °C. Finally, the $\phi$-scan around the [1 1 $\bar{2}$ 1] direction of YMO (Fig. 3b, top) displays six peaks. The in-plane epitaxial relationship to Pt is found to be the same as in the previous case.

We present in Fig. 4 the sketches of the epitaxial relationships of the Pt(1 1 1) surface on (a) ALO(0 0 0 1) and (b) STO(1 1 1). The ALO(0 0 0 1) lattice (Fig. 4a) presents an in-plane parameter $a_{ALO} = 4.75$ Å whereas for Pt(1 1 1) the in-plane parameter is $a_{Pt} = 2.77$ Å. The distance denoted by $L$ corresponds to $a_{ALO} \cdot \sqrt{3}$ and it matches with the distance $3a_{Pt}$. In this arrangement, the lattice mismatch is 1.0%, and the Pt film is expected to be compressively stressed as observed in the thinnest films (Fig. 2). Next, in Fig. 4b we consider the epitaxy of Pt(1 1 1) on STO(1 1 1). The in-plane parameter of the $SrTiO_3$ is 2.76 Å, close to the 2.77 Å for Pt. In these conditions, Pt film is expected to growth with a low compressive lattice mismatch of 0.4%. Finally, we turn to the YMO/Pt epitaxy. In Fig. 4c is depicted the YMO(0 0 0 1) surface corresponding to a manganese oxide termination, although the arguments presented are also suitable for yttrium oxide termination. The primitive cell in the hexagonal YMO has an in-plane parameter of 6.15 Å. This distance does not commensurate with the 2.77 Å parameter of Pt. When considering the distances between nearest neighbors of ions along the [1 $\bar{1}$ 0 0] direction, $L_0$, an average in-plane interatomic distance can be defined as 3.54 Å. In the bottom sketch of Fig. 4c, we represent the manganese atoms ordering along the [1 $\bar{1}$ 0 0] YMO direction, and the Pt atoms ordering along the [1 $\bar{1}$ 0] direction. The arrangement suggests that a multicell matching occurs where four cations in the YMO film are related to five atoms of the Pt network and, in this situation, the lattice mismatch is 2.09%. However, we note that this lattice mismatch is evaluated at room temperature. YMO is deposited at 800 °C, and it has to be mentioned that its lattice expansion coefficient can differ notably to those of a metal (Pt). Although the proposed epitaxial model fits well at room temperature, alternative arrangements may occur during growth at high temperature, suggesting that the cooling process after the film growth can play an important role.

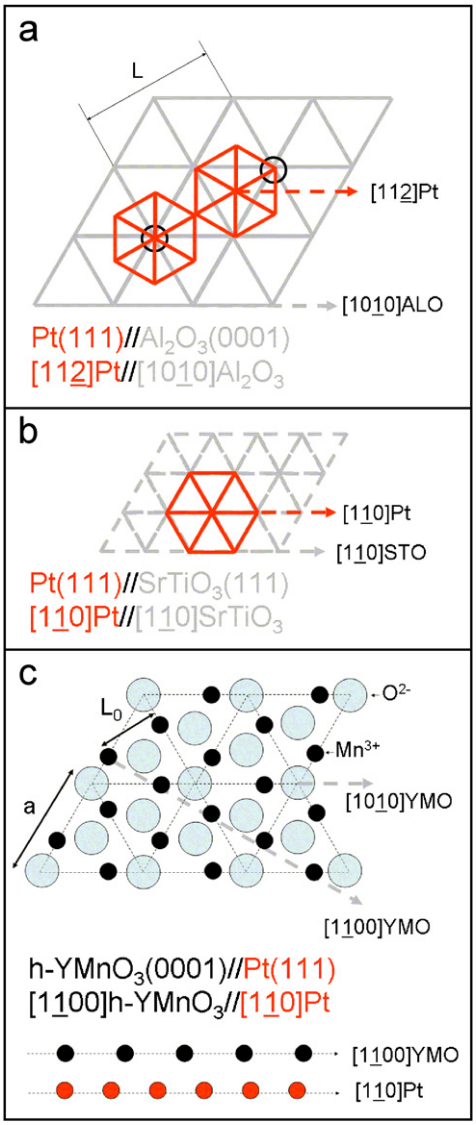


Fig. 4. Sketch of arrangement of atoms according to the epitaxial relationships for: (a) Pt(1 1 1)//$Al_2O_3$(0 0 0 1), (b) Pt(1 1 1)//$SrTiO_3$(1 1 1) and (c) $YMnO_3$(0 0 0 1)//Pt(1 1 1).

Topographic AFM images from Pt electrodes and YMO films are shown in Fig. 5. Panels (a) and (b) correspond to Pt electrodes (15.8 nm thick) on STO(1 1 1) and ALO(0 0 0 1), respectively. Although the thickness of the Pt films is low, the original substrate morphology of terraces and steps is not preserved. Instead of it, there are islands with a lateral size up to around 100 nm. Detailed observation and height profile measurements indicated that they are two-dimensional (2D) islands, 1 u.c. high, formed on preexisting ones. Thus, they are multilayer (mound-like type) islands, which are reported to form in the epitaxy of metals [11] and also of oxides [12]. They form when the growth of a film by a layer-by-layer mechanism is limited by an energy barrier that reduces the probability of an adatom to jump from a 2D island to the bottom layer [13].

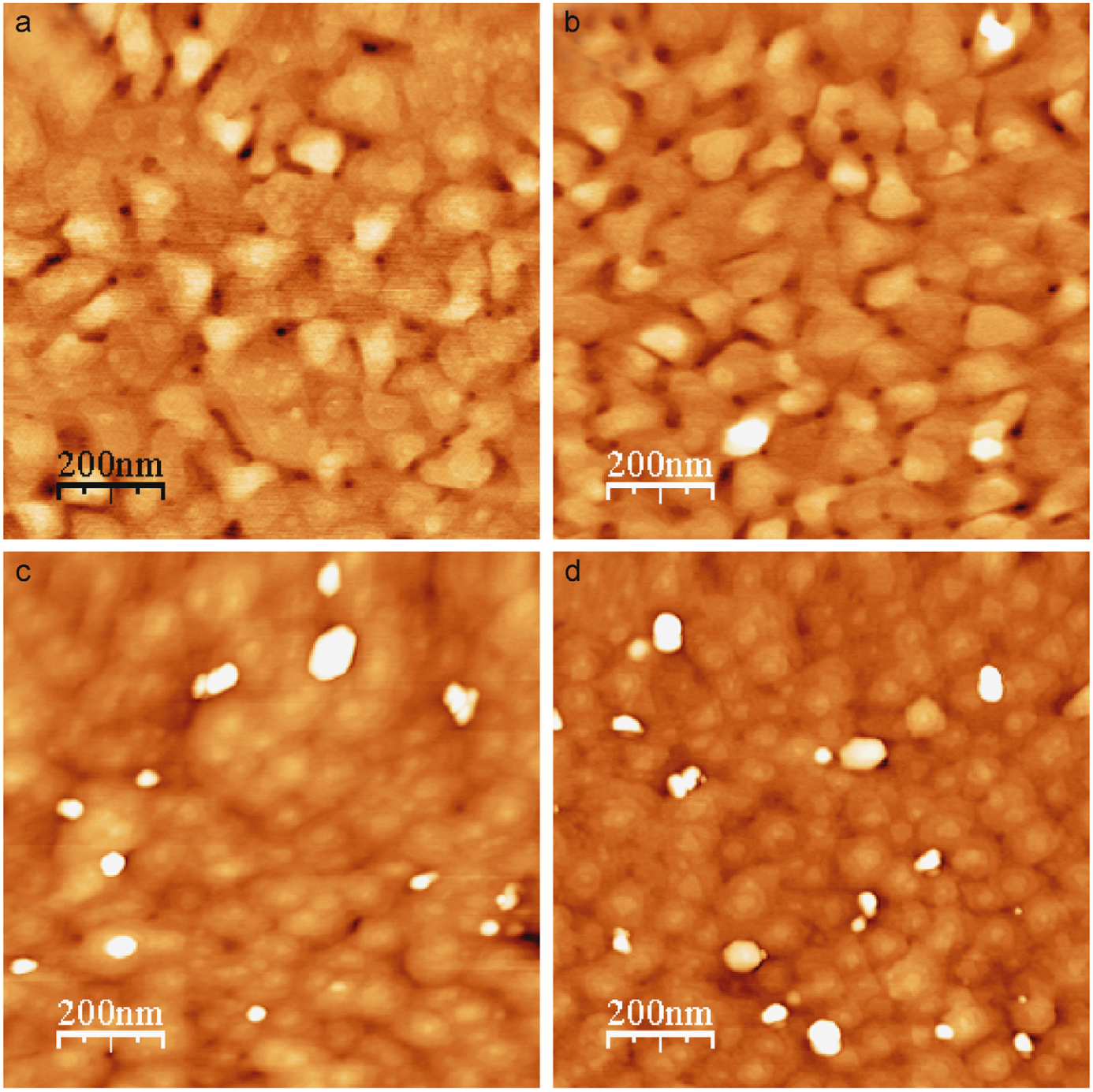


Fig. 5. Atomic force microscopy topographic images ($600 \times 600\,nm^2$) of Pt films 15.8 nm thick on (a) $SrTiO_3$(1 1 1) and (b) $Al_2O_3$(0 0 0 1), and of $YMnO_3$ films 150 nm thick on Pt covered (45 nm thick) (c) $SrTiO_3$(1 1 1) and (d) $Al_2O_3$(0 0 0 1).

This favors nucleation of 2D islands on preexisting ones before their coalescence and thus multilayered islands form. Characterization of films with varied thickness revealed (not shown here) a progressive increase in mound height and lateral size with thickness. This morphology evolution resulted in a progressive increase of the film roughness with thickness, raising the root-mean-square roughness almost linearly from around 0.5 nm (for the $t = 15.8$ nm films shown in Fig. 5a and b) to above 1.5 nm for 180 nm thick films. The topographic AFM images of the YMO films (100 nm thick) grown on Pt-coated STO(1 1 1) and ALO(0 0 0 1) (Fig. 5c and d, respectively) also show multilayered islands. The images also reveal the presence of particulates and nanocrystals, some of them hexagonally shaped. The crystals can be up to around 100 nm long and up to more than 10 nm high.

In order to get a better insight into the crystallographic properties of these heterostructures, a high-resolution transmission electron microscopy (HRTEM) study has been carried out on a YMO/Pt/STO(1 1 1) sample. In the

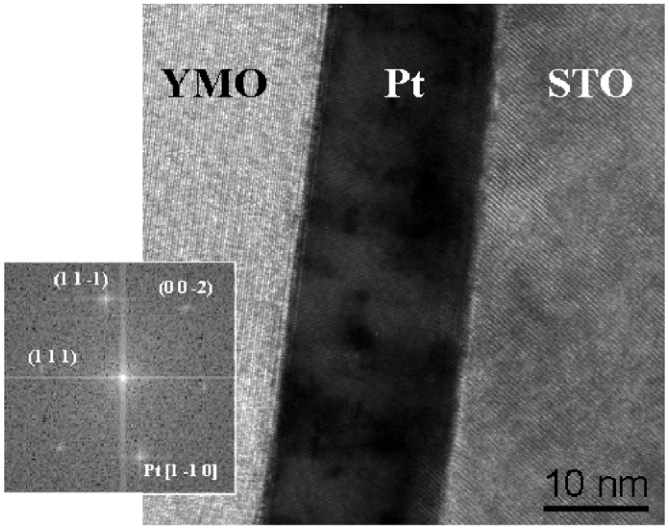


Fig. 6. HRTEM image showing the $YMnO_3$/Pt/STO heterostructure and power diffraction of the highlighted zone in the Pt buffer layer along the [1 $\underline{1}$ 0] zone axis.

cross-section image of Fig. 6, it can be appreciated that the Pt buffer layer has a thickness of about 15.8 nm, in good agreement with data extracted from X-ray analysis and a (1 1 1) texture as revealed in the corresponding power diffraction by Fast Fourier Transform (FFT) in the inset. In the higher resolution images of Fig. 7 (panels a and b), it can be appreciated that the interfaces YMO/Pt and Pt/STO appear to be sharp. The epitaxial relationships derived from the FFT corresponding to the different layers are in agreement with XRD analysis. In the explored region, the YMO appears to be of high crystal quality. The stacking of $MnO_5$ and $YO_7$ polyhedral layers along the [0 0 0 1] direction is perfectly resolved in the zoom as shown in Fig. 7c. We note, however, that this crystal quality contrasts with the broadening observed in the rocking curves and the presence of nanocrystals described above. However, since the observable region extended along a few hundreds of nanometers, the existence of a certain disorder at a longer range cannot be ruled out. Detailed lower magnification plane view examination

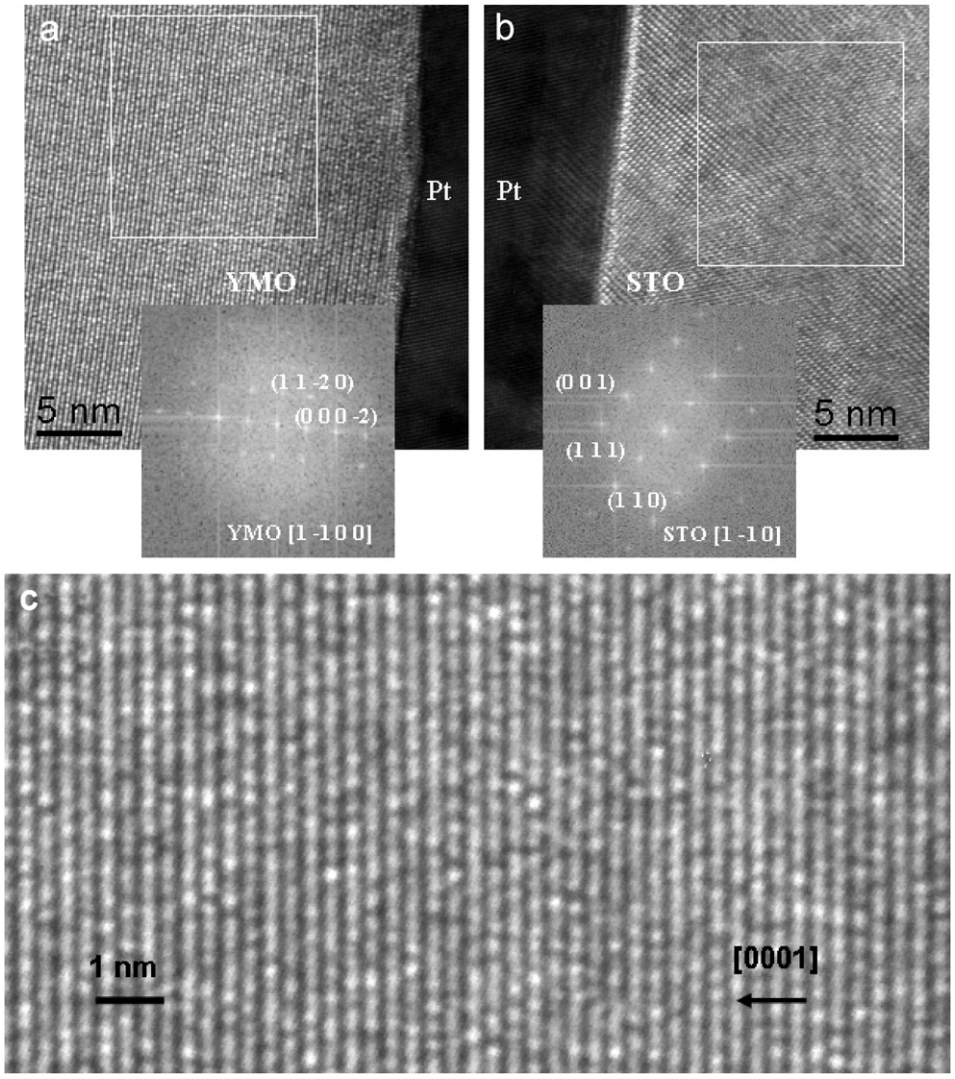


Fig. 7. HRTEM images showing the $YMnO_3$/Pt (a) and Pt/STO (b) interfaces, with the corresponding FFT images along the [1 $\underline{1}$ 0] zone axis. (c) Zoom of part (a) showing the stacking of $MnO_5$ and $YO_7$ layers along the [0 0 0 1] $YMnO_3$ direction.

under diffraction contrast imaging conditions will clarify the microstructure.

## 4. Summary

In summary, epitaxial (1 1 1) Pt films on STO(1 1 1) and ALO(0 0 0 1) substrates have been grown with a low roughness surface. YMO films deposited on the Pt(1 1 1) electrodes are (0 0 0 1) textured. We have determined the in-plane epitaxy and we have shown the coexistence of two Pt domains, 60° rotated, on the corresponding substrates. Due to the two-domain structure found in the epitaxy of Pt on both the used substrates, epitaxial YMO films are most likely to be also formed by two domains. A simple atomistic picture has been used to describe the origin of the observed epitaxial relationships. In spite of the fact that the HRTEM shows abrupt interfaces and high-quality epitaxial layers in the observable region of the YMO/Pt/STO(1 1 1) sample, the rocking curves and the presence of nanocrystals suggest the existence of a certain disorder in the film. The experimental observation of a multidomain structure of YMO in the YMO/Pt bilayers may have severe implications in functional properties of YMO.

## Acknowledgments

Financial support by the MEC of the Spanish Government (projects NAN2004-9094-C03 and MAT2005-5656-C04), and FEDER and the STREP project MaCoMuFi (FPG-033221) of the E.U. are acknowledged.

## References

[1] M. Fiebig, J. Phys. D: Appl. Phys. 38 (2005) R123; W. Prellier, M.P. Singh, P. Murugavel, J. Phys.: Condens. Matter. 17 (2005) R803.
[2] V. Laukhin, V. Skumryev, X. Marti, D. Hravobosky, F. Sanchez, M.V. García-Cuenca, C. Ferrater, M. Varela, U. Lüders, J.F. Bobo, J. Fontcuberta, Phys. Rev. Lett. 97 (2006) 227201.
[3] B.B. van Aken, T.T.M. Palstra, A. Filippetti, N. Spalding, Nat. Mater. 3 (2004) 164.
[4] A. Muñoz, J.A. Alonso, M.J. Martínez-Lope, M.T. Casáis, J.L. Martínez, M.T. Fernández-Díaz, Phys. Rev. B 62 (2000) 9498.
[5] D. Ito, N. Fujimura, T. Yoshimura, T. Ito, J. Appl. Phys. 93 (2003) 5563.
[6] J. Dho, M.G. Blamire, Appl. Phys. Lett. 87 (2005) 252504.
[7] J. Dho, C.W. Leung, J.L. MacManus-Driscoll, M.G. Blamire, J. Crystal Growth 267 (2004) 548.
[8] S. Ramanathan, B.M. Clamans, P.C. McIntyre, U. Dahmen, Phil. Mag. A 8 (2001) 2073.
[9] D.O. Klenov, T.R. Taylor, S. Stemmer, J. Mater. Res. 19 (2004) 1477.
[10] A.A. Asthagiri, C. Niederberger, A.J. Francis, L.M. Porter, P.A. Salvador, D.S. Sholl, Surf. Sci. 537 (2003) 134.
[11] J.A. Stroscio, D.T. Pierce, M.D. Stiles, A. Zangwill, L.M. Sander, Phys. Rev. Lett. 75 (1995) 4246.
[12] F. Sánchez, I.C. Infante, U. Lüders, Ll. Abad, J. Fontcuberta, Surf. Sci. 600 (2006) 1231.
[13] M.G. Lagally, Z. Zhang, Nature 417 (2002) 907.